ELSEVIER

NeuroImage

www.elsevier.com/locate/ynimg
NeuroImage xx (2005) xxx – xxx

A consistent relationship between local white matter architecture and functional specialisation in medial frontal cortex

T.E.J. Behrens,* M. Jenkinson, M.D. Robson, S.M. Smith, and H. Johansen-Berg

Oxford Centre for Functional Magnetic Resonance Imaging of the Brain, University of Oxford, John Radcliffe Hospital, Oxford OX3 9DU, UK

Received 10 June 2005; revised 7 September 2005; accepted 13 September 2005

Functionally significant landmarks in the brain do not necessarily align with local sulcal and gyral architecture in a manner that is consistent across individuals. However, the functional specialisation underlying these landmarks is strongly constrained by the *connectional* architecture of the region. Here, we explore this relationship in the supplementary motor area (SMA) and pre-SMA in the medial frontal cortex of the human brain. Using diffusion tensor, conventional and functional MR imaging, we find that the location of the functional boundary between SMA and preSMA is more consistent with respect to specific features of the local white matter as it approaches neocortex than with respect to the local gyral and sulcal anatomy in the region.

Introduction

Our understanding of functional architecture in the brain relies upon our ability to localise neural responses with respect to known regions of functional specialisation. It has been convenient to assume that these functional regions can be identified on the basis of the gross sulcal and gyral anatomy. However, recent studies have demonstrated that boundaries between regions of distinct cyto- and receptor architecture, which have direct influence on functional specialisation, do not necessarily align with local landmarks in the gross anatomy (e.g., Amunts et al., 1999).

Even in the absence of a correspondence between function and gross anatomy in the brain, a relationship is expected between regional function and local *connectional* architecture. Anatomical connections constrain the nature of information available to a region and the influence that it can exert over other regions in a distributed network. Connectional anatomy can be expected to determine local functional organisation (Passingham et al., 2002).

Magnetic Resonance diffusion tensor imaging (DTI) (Basser et al., 1994) is a new technique, which allows features of local white matter architecture to be inferred from diffusion properties. For example, the dominant local diffusion orientation is thought to align well with the mean local fibre orientation (Beaulieu and Allen, 1994), and the *anisotropy* of local diffusion (FA) is thought to reflect factors such as the degree of myelination and cellular packing density of local white matter (Beaulieu, 2002). Recent research using DTI has revealed that connectional boundaries in diffusion data parallel functional boundaries both in subcortical (Behrens et al., 2003; Wiegel et al., 2003) and cortical (Johansen-Berg et al., 2004a) grey matter.

In Johansen-Berg et al. (2004a), we used diffusion-based tractography to find a connectional boundary between two functionally distinct regions in medial frontal cortex. The supplementary motor area (SMA) is involved in motor tasks (Tanji, 2001) and connects to motor regions including precentral gyrus, ventro-lateral thalamus and cortico-spinal tract (Luppino et al., 1993; Maier et al., 2002; Matelli and Luppino, 1996). The preSMA is located proximal but anterior to SMA in medial area BA6. It is involved in more cognitive tasks, albeit including cognitive aspects of movement control and motor learning (Hikosaka et al., 1996; Matsuzaka and Tanji, 1996; Picard and Strick, 1996) and connects to prefrontal and medial parietal regions (Johansen-Berg et al., 2004a; Luppino et al., 1993). In diffusion tractography data from medial frontal cortex, we found clusters of voxels with markedly different anatomical connectivity patterns (Johansen-Berg et al., 2004a). These clusters corresponded to areas which, using functional MRI, were found to be active during motor (SMA) or cognitive (preSMA) tasks. Here, we test whether there is a relationship between the SMA/preSMA boundary defined functionally, and the local white matter architecture in the region. We hypothesise that the local fibre orientations will predict the boundary between the two regions. We find that this functional boundary lies in a consistent location with respect to features of the diffusion tensor data such as the local fibre orientations but not with respect to the local sulcal and gyral anatomy. We go on to show that if information about local fibre orientation is incorporated in the inter-subject alignment process, the alignment of the *functional* boundary across subjects is improved.

* Corresponding author. Fax: +44 1865 222717.
E-mail address: behrens@fmrib.ox.ac.uk (T.E.J. Behrens).
Available online on ScienceDirect (www.sciencedirect.com).

1053-8119/$ - see front matter © 2005 Elsevier Inc. All rights reserved.
doi:10.1016/j.neuroimage.2005.09.036

Methods

Data acquisition

We used the same diffusion-weighted data, BOLD fMRI data and T1-weighted images from 9 healthy subjects (ages 24–35, 5 male, 4 female) as described previously (Johansen-Berg et al., 2004a). Data were acquired on a 1.5 T Siemens Sonata MR scanner with a maximum gradient strength of 40 mTm^{-1}. All subjects gave informed written consent in accordance with ethical approval from the Oxford Research Ethics Committee.

Diffusion-weighted data

Diffusion-weighted data were acquired using echo planar imaging (72 × 2 mm thick axial slices, matrix size 128 × 104, field of view 256 × 208 mm^2, giving a voxel size of 2 × 2 × 2 mm^3). Signal to noise ratio in the raw T2-weighted maps was approximately 14 in brain tissue. The diffusion weighting was isotropically distributed along 60 directions using a b-value of 1000 s mm^{-2}. For each set of diffusion-weighted data, 5 volumes with no diffusion-weighting were acquired at points throughout the acquisition. Three sets of diffusion-weighted data were acquired for subsequent averaging to improve signal to noise ratio. The total scan time for the DWI protocol was 45 min.

BOLD fMRI data

BOLD fMRI data were acquired using echo planar imaging (20 × 5 mm thick axial slices positioned to cover the top portion of the brain, matrix size 128 × 128, field of view 256 × 256 mm^2, giving a voxel size of 2 × 2 × 5 mm^3, TR = 2.5 s, 341 volumes, TE = 45 ms, flip angle = 90°). Subjects were given instructions and practice on the fMRI tasks before entering the scanner. Blocks (30 s duration) of rest (A) alternated with blocks of finger tapping (B) or serial subtraction (counting backward in threes) (C) in a 3.5 times repeated ABACACAB cycle. The current task was indicated by the word 'rest', 'move' or 'count' displayed on a projection screen at the foot of the scanner bed viewed via a mirror. During 'move' blocks, subjects were trained to press buttons with the fingers of their right hand in a repeating 1234321 sequence at a frequency of approximately 4 Hz. During 'count' blocks, subjects were instructed to count covertly backwards in threes from a three digit reference number that was displayed on the screen for 2 s before the start of the counting block. To ensure task compliance, at the end of each counting block, a red screen instructed subjects to report the number they had reached by pressing buttons with their index figure to indicate tens and middle finger to indicate units (e.g., if they had reached 47, they would press the index finger button 4 times and the middle finger button 7 times). The total scan time for the FMRI protocol was approximately 15 min.

A T1-weighted

A T1-weighted anatomical image was acquired using a FLASH sequence (TR = 12 ms, TE = 5.65 ms, flip angle = 19°, with elliptical sampling of k-space, giving a voxel size of 1 × 1 × 1 mm^3 in 5:05 min).

Data analysis

Diffusion-weighted data

Diffusion-weighted data were corrected for eddy currents and head motion using affine registration to a reference volume (Jenkinson and Smith, 2001). Data from the three acquisitions were averaged to improve signal to noise. Diffusion tensors were reconstructed at each voxel using FDT (FSL, http://www.fmrib.ox.ac.uk/fsl.).

BOLD fMRI data

BOLD fMRI data were analysed using tools from FSL (www.fmrib.ox.ac.uk/fsl). The following preprocessing steps were applied: motion correction using MCFLIRT; removal of nonbrain structures using BET (Smith et al., 2002); spatial smoothing using a Gaussian kernel of FWHM 3 mm; mean-based intensity normalisation of all volumes by the same factor; temporal high pass filtering using Gaussian-weighted least squares fitting with a filter of sigma = 57.5 s. Time series statistical analysis was carried out using FILM with local autocorrelation correction (Woolrich et al., 2001).

Locating the functional boundary between SMA and preSMA

Considering only a region of interest in medial frontal cortex which included both SMA and preSMA (Fig. 1), we formed a mask of all voxels which activated during either 'count' or 'move' blocks, when compared to rest, with an uncorrected false positive rate P = 0.05 (z = 2.3). In these voxels, we subtracted the signal change apportioned to 'move' from that apportioned to 'count', attaching a value of zero to voxels which did not activate significantly during either task (Fig. 2, left). Observing that the functional boundary lay predominantly in the coronal plane, we summed this signal within the region of interest along the left–right (x) and inferior–superior (z) axes leaving a functional profile along the anterior–posterior axis (y), perpendicular to the plane of the boundary (Fig. 2, right). In each of nine subjects, this functional profile changed from negative ('move' > 'count') to positive ('count' > 'move') when moving anteriorly along the posterior–anterior axis. We defined the functional boundary between SMA and preSMA as the point at which this profile crossed the zero line. The location of this boundary in the nine subjects was distributed around the vertical line from the anterior commisure (y = 0 mm in MNI space; Evans et al., 1992), as expected from previous studies of cytoarchitecture in the region (Zilles et al., 1996).

Alignment of functional, diffusion and T1-weighted data within subject

Within each subject, affine transformation matrices were computed between an example volume from the functional

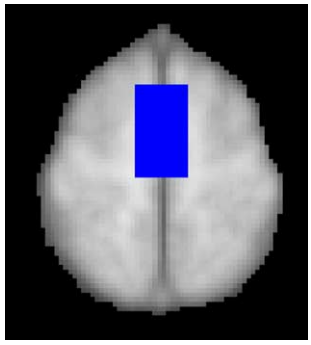

Fig. 1. Axial section through the region of interest used for the SMA/pre-SMA analyses. The limits of the ROI in MNI152 space were: x = [−10, 10] mm, y = [− 20, 18] mm on 3 axial slices: z = [58, 60, 62] mm.

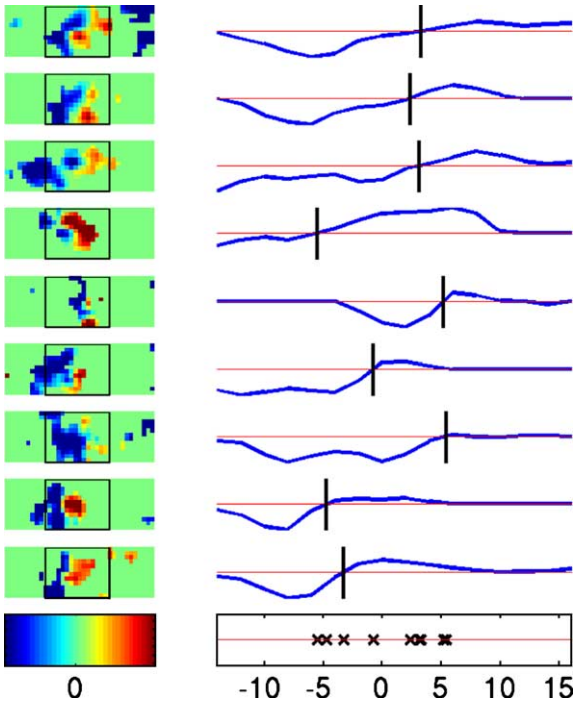

Fig. 2. Functional boundaries between SMA and preSMA in 9 subjects after alignment according to global brain shape. Left: contrast between 'count' blocks and 'move' blocks in a single axial slice through the region of interest in medial frontal cortex. Blue shows areas in which 'move' > 'count' (SMA). Red shows areas in which 'count' > 'move' (preSMA). Values are shown only in voxels activated during either 'count' or 'move' blocks with an uncorrected false positive rate $P = 0.05$ ($z = 2.3$). Right: data taken from within the black rectangles, summed across slices and along the left–right axis (up–down in left hand column of figure) leaving a functional profile along the anterior–posterior axis. (For interpretation of the references to colour in this figure legend, the reader is referred to the web version of this article.)

series and the T1-weighted image, and between a T2-weighted image with no diffusion weighting in the space of the diffusion images and the T1-weighted image (Jenkinson and Smith, 2001). With the exception of areas which suffer from susceptibility related distortions in EPI data (which do not include the SMA/preSMA region), the functional, diffusion and T1-weighted data were assumed to be aligned for the remainder of the analysis.

Alignment of data across subjects: testing for correspondence between functional, anatomical and connectional features

We used 3 separate criteria for aligning data between subjects: global brain shape; local gyral and sulcal anatomy; and local white matter architecture. For the global alignment, the alignment target was the MNI152 brain. For the local alignments, the alignment target was the data from the single subject whose functional boundary was closest to MNI $y = 0$. After aligning the subjects on the basis of each criterion, we computed the variability across the subjects in the location of the functional boundary.

In each subject, T1-weighted data were first aligned to the MNI152 average brain (Evans et al., 1992) using affine registration. This same affine transformation was applied to the FMRI and DTI data. Diffusion tensors were reoriented to maintain the orientations of their first eigenvectors (Alexander et al., 2001). At the end of this step, data were considered to be aligned across subjects on the basis of their global brain shape. We then tested whether the incorporation of local connectional or anatomical features could further improve alignment of the functional boundaries: The geometry of medial area 6 is such that the boundary between SMA and preSMA lies predominantly in the coronal plane; we therefore searched for a single translation of the data in the anterior–posterior axis (y) perpendicular to this plane within a small region of interest including the SMA and preSMA (Fig. 1). Two sources of data were considered for performing this refinement of the initial global result.

- Searching for a translation which best matched the T1-weighted data within this region was considered to align subjects according to their local gyral and sulcal anatomy as visible in the MRI data.
- Searching for a translation which best matched the diffusion tensor data in this region was considered to align subjects according to features of their connectional architecture.

In order to find the best translation to match a source and target image, we shift the source image along the y-axis by an integer number of voxels. We then compute the value of an "objective function" (see below) between these candidate aligned images, in the region of overlap between the ROIs in the two images. We repeat this for every possible shift that leaves more than 4 overlapping voxels in the y-direction. The candidate shift that results in the greatest value of the objective function in question is taken to be the optimal shift to align the images. Different choices of objective function, using different data, will optimise the alignment for different anatomical features (see below).

Objective functions for local data alignment

For each type of data, we defined two objective functions which we sought to maximise to find the optimal image alignment. The different objective functions will aim to match different features between the images.

T1-weighted data

Local alignment of the T1-weighted images was carried out using two possible objective functions: normalised correlation, which considers voxels independently; and mutual information which considers a statistic on the joint histogram of the two images to be aligned. For details, see Jenkinson and Smith (2001). These objective functions are based only on the image intensity values at each voxel in the T1-weighted scans, and will aim preferentially to align gross structure in the images such as the sulcal and gyral anatomy.

Diffusion tensor data

We also considered two objective functions for local alignment of the diffusion tensor images. First, we used the tensor scalar product described in Alexander et al. (1999). This function aims to match the tensors at each voxel for overall volume, for diffusion anisotropy and for dominant orientation. The similarity between two images I1 and I2 is considered to be:

$$S(I_1,I_2) = T(I_1,I_2)/Z \quad (1)$$

where

$$T(I_1,I_2) = \sum_{v=1}^{V}\left[\sum_{i=1}^{3}\sum_{j=1}^{3} D_{ij}^{1}(v)D_{ij}^{2}(v)\right],$$

V is the number of voxels in each image, D_{ij}^{1} is the ijth element of the diffusion tensor at voxel v in image I_1, and Z is the normalisation constant $Z = \sqrt{T(I_1,I_1) \times T(I_2,I_2)}$.

As described above, this objective function considers not only the anisotropy and orientation of the tensors at each voxel, but also their absolute diffusivities (which are related to the volume of the tensor). The diffusivity of water varies very little within brain parenchyma, but varies by a factor of approximately 3 between tissue and cerebro-spinal fluid (CSF). Considering absolute diffusivities will bias the objective function to prefer alignments which match the boundaries between brain tissue and CSF; i.e., this objective function will aim to match gyral and sulcal architecture.

The second DTI objective function is identical to the first with the exception that each tensor is first normalised by the geometric mean of its eigenvalues. The tensors then have equal volume (regardless of their original absolute diffusivity). This objective function will aim to match images such that anisotropic regions with similar diffusion orientations are well aligned, implicitly weighting diffusion direction with anisotropy before performing comparisons, i.e., this second DTI-based objective function will seek to align images on the basis of their local white matter architecture.

Results

Testing for functionally relevant features in local diffusion and anatomical data

Fig. 3 shows DTI data in an axial slice of the medial frontal region of interest in nine subjects. The functional boundaries are overlaid as green lines on each subject. Using these data, in each subject, we formed a separate image of each of the x, y and z components of the principal diffusion direction modulated by the fractional anisotropy (Pierpaoli and Basser, 1996) at each voxel. For example, in the resulting scalar image for the x direction, high voxel values indicate that the principal diffusion direction is closely aligned with the x-axis and diffusion in that voxel is strongly anisotropic.

To test for consistency across subjects in the spatial distribution of these features when subjects are aligned for global brain shape, from these images we formed a profile along the anterior–posterior axis similar to the functional profiles described in the previous section, but separately for each hemisphere. These profiles exhibited little consistency across subjects (e.g., for the ROI considered in the right hemisphere, the means of the correlations of each of the three profiles between every pair of subjects were 0.06, −0.01 and 0.05 for x, y and z components of the principal diffusion direction, respectively. Top left in Fig. 4 shows the x profiles. y and z profiles were similar). To test whether local diffusion features are more consistent following functional alignment, we then translated the data from each subject in the anterior–posterior axis such that the functional boundary derived in the previous section occurred at $y = 0$. After realignment of the subjects on the basis of their functional boundaries, the diffusion-based profiles relating to the x and z components of the principal diffusion direction exhibited significantly increased consistency across subjects ($P < 0.001$ for x, $P < 0.05$ for z) (the mean correlations between the functionally aligned diffusion profiles were 0.21, −0.05 and 0.15 for x, y and z components of the principal diffusion direction, respectively. Top right in Fig. 4 shows the functionally aligned x profiles at the axial level chosen in the right hemisphere. The functionally realigned z profiles also showed high consistency. No structure was visible in the realigned y profiles.).

To account for potential asymmetries of the functional boundaries, and to ensure that effect did not depend on the

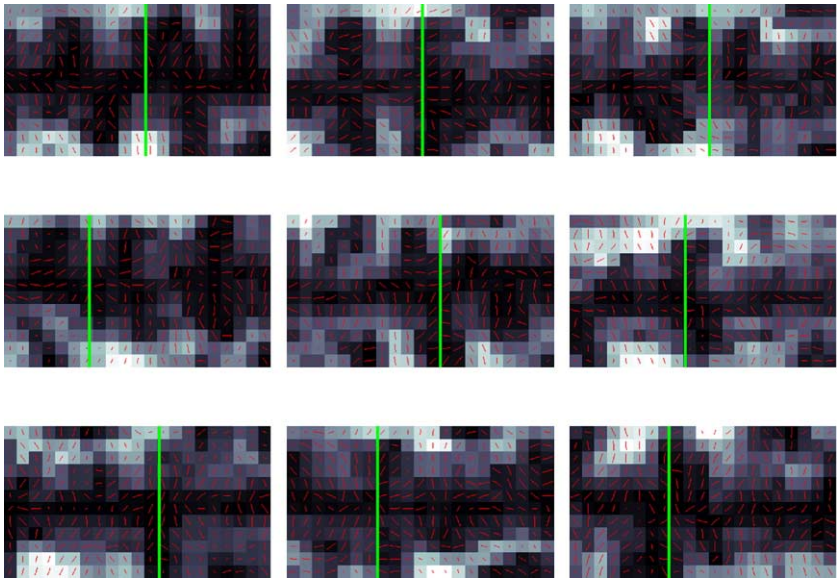

Fig. 3. DTI data in nine subjects. For each subject, data are shown from a single axial (xy) slice through the region of interest in medial frontal cortex. Fractional anisotropy images are shown in grey scale. Projections of the principal diffusion direction into the axial plane are overlaid in red. The positions of the functional boundaries between SMA and preSMA are shown as green lines through the axial section. (For interpretation of the references to colour in this figure legend, the reader is referred to the web version of this article.)

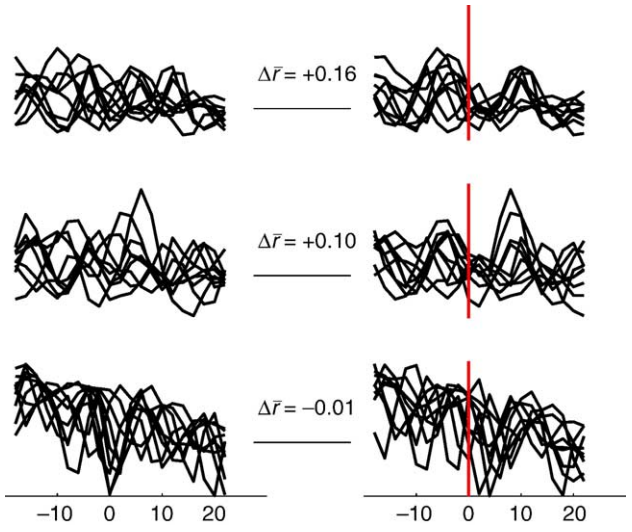

Fig. 4. Relationships between structure and function. Profiles are taken through the DTI (top and middle) and T1-weighted (bottom) data. In each case, the graph on the left shows the profiles aligned in order to match global brain shapes and the graph on the right shows the profiles aligned such that the functional boundaries appear at the same location on the anterior–posterior axis ($y = 0$, red line). The DTI profiles shown are the x (top) and z (middle) profiles in the right hemisphere. Numbers between left and right columns show the increase in average correlations between profiles from every pair of subjects after the functional boundaries are aligned. The DTI profiles exhibit greater consistency between subjects when aligned to match functional boundaries. No such characteristic profile is visible in the T1-weighted data (see main text). (For interpretation of the references to colour in this figure legend, the reader is referred to the web version of this article.)

specific geometry of the anatomy at the axial level in question, we then computed the locations of the functional boundaries separately within each hemisphere for ROIs two slices thick, taken at three separate axial levels within the SMA/pre-SMA (z = [52−56, 56−60, 60−64] mm). We computed the diffusion profiles exactly as above but considering data in these same single-hemisphere ROIs. We then shifted the diffusion profiles from each hemisphere at each axial level, according to boundaries defined in the functional data in that same hemisphere at that axial level. Consistency across subjects in the x and z diffusion profiles across subjects was increased after alignment of the functional boundaries in all cases (this was significant in 3 out of 6 x profiles and 4 out of 6 y profiles). This result suggests that features of the local connectional architecture visible in the diffusion tensor data contain information about the location of the functional boundary between SMA and preSMA.

The same approach was taken with the T1-weighted *structural* data. In each subject, an anterior–posterior structural profile was formed in each hemisphere by summing voxel signal intensities in the T1-weighted images along the left–right and inferior–superior axes. Unlike the diffusion data, these structural profiles exhibited some consistency in their gross features even when aligned only on the basis of global brain shape (for example, the right hemisphere profiles are shown bottom left in Fig. 4—mean correlation of 0.34 between profiles). However, the structural profiles showed no increase in cross-subject consistency after realignment according to the location of the functional boundaries (right hemisphere profiles are shown in right hand column in Fig. 4 (b)—mean correlation of 0.33 between profiles). As with the diffusion data, hemisphere specific functional shifts were applied at the same three axial levels. There was no case of a significant increase in the consistency across subjects, suggesting that the local gyral and sulcal anatomy does not provide additional information about the location of the functional boundary.

Functional realignment increased the correlation between subjects in their connectional, but not structural profiles between subjects. However, the reader should note that the structural profiles started with a higher mean correlation (due to a slight trend in intensity from posterior to anterior that was consistent across subjects). Also, the original alignment into the MNI reference frame was performed with affine registration of the structural images. It is possible therefore, that a subsequent increase in correlation would have been harder to achieve in the structural profiles than in the connectional profiles. In the next section, we address this concern by effectively performing the experiment in reverse. We search for the translations that best match both the diffusion, and functional data sets, and compare these translations with those required to match the functional boundaries.

Structural realignment of functional boundaries

The results from the previous section suggest that functional boundaries align more consistently with local white matter architecture than with local gyral and sulcal anatomy. In this section, we will test whether this same local connectional architecture predicts the functional boundaries better than position with respect to global brain shape. If this is the case, then it should be possible to use information in the local diffusion tensors to align the data such that the variability across subjects in the location of the functional boundary is lower than can be achieved using either the global or local information in the T1-weighted images.

Starting from data which were aligned using affine registration (Jenkinson and Smith, 2001) to match their global brain shape, we chose two potential criteria for further aligning the diffusion tensor data (see Methods). The first aims to match the diffusion tensors at each voxel for overall volume, shape and orientation. The second is identical to the first except that before comparison, the tensors are normalised to unit volume, so that the absolute diffusivity has no effect on the registration. This is an important distinction. In the first case, when the absolute diffusivity is considered, the dominant consideration for matching diffusion tensor images will be the location of the cerebro-spinal fluid (CSF) whose diffusivity is approximately a factor of 3 bigger than the diffusivity of brain tissue. By matching the location of the CSF, this objective function will match the sulcal and gyral architecture. In the case of the objective function that does not consider the absolute diffusivity, images are matched on the orientation and anisotropy of the diffusion tensors; the dominant consideration will be given to matching regions of high anisotropy; and in particular to matching the orientation of the principal axis of diffusion within such regions. That is, this second objective function will aim to match local white matter architecture. We used these two objective functions to compute the shift along the anterior–posterior axis which best matched subjects according to their diffusion tensor data in the local region of interest.

We also considered this same region of interest in the T1-weighted data to see whether local gyral and sulcal anatomy could predict the location of the functional boundary. We performed this test using both automatic and manual registration techniques. In the automatic alignment, looking at the ROI in question, we searched

for the anterior–posterior shift between subjects which minimised each of two commonly used objective functions for scalar data (see Methods and Jenkinson and Smith, 2001). In the manual alignment, we showed 2 experienced neuroanatomists the location of the functional boundary in the structural ROI from one randomly selected subject. We then asked them to identify a corresponding anatomical location in each of the 8 other subjects. We then shifted the data so that these anatomical locations lined up. If either the automatic or the expert manual registration were to reduce the variability in the location of the functional boundaries, we would conclude that gyral and sulcal anatomy exhibited consistency across subjects with respect to the functional boundary of interest.

In all cases, the alignment process is only able to consider very local information. Therefore, in each case, if the data did not contain information pertinent to the location of the functional boundary, then the alignment process would have less information about this location than was available to the global affine alignment. Hence, refining the global alignment according to this local objective function would increase the between-subject variability in the boundary location. However, if functionally relevant local information was represented in the objective function, then the location of the functional boundary might be expected to be less variable between locally than globally aligned subjects.

We measured the variability across subjects in the location of the functional boundary between SMA and preSMA after alignment on the basis of global brain shape alone and again after each of the local realignments. The following realignments increased this functional variability (Table 1): realignment by each of the automatic objective functions based on the local T1-weighted data; manual realignment by each of the experienced neruoanatomists working with the local T1-weighted data and automated registration based on the first of the DTI objective functions (which was dependent on the absolute diffusivity at each voxel). In each of these cases, without access to brain boundary information in the local region of interest, the cost functions would aim to match subjects based on their local gyral and sulcal architecture.

The only local realignment that reduced variability between subjects in the location of the functional boundary was the automated realignment by the second DTI-based objective function (which depended only on the orientation and anisotropy of local diffusion) ($P < 0.1$, Table 1).

Fig. 5 shows that there is a clear relationship between the relative shifts which best align the functional boundaries across subjects, and the relative shifts which best align the second DTI-based cost function "DTI2" (left) ($r^2 = 0.6$). By contrast, there is no clear relationship between functional shifts and the shifts which optimise either of the T1-weighted objective functions ($r^2 = -0.0003, -0.0002$), or with the shifts defined by either of the manual alignments ($r^2 = 0.10, 0.08$).

Discussion

We have found that the functional boundary between SMA and preSMA is more easily predicted on the basis of connectional architecture visible in diffusion-tensor images, than on the basis of gross anatomy visible in T1-weighted MR images. We have gone on to show that the existence of functionally relevant features in DTI data can be used to better align functional landmarks across individuals.

This finding is consistent with the notion that the function of a grey matter region is influenced not by its physical location in cortex but by its connectional position with respect to others in a distributed network of regions (Passingham et al., 2002). Different functional regions may therefore be distinguished by features of their connectivity (Johansen-Berg et al., 2004a,b).

It is not trivial to discern which particular image feature drives an alignment process, but our pilot studies suggest distinguishable features in the white matter approaching SMA and preSMA. All of the white matter approaching the medial superior cortical surface is oriented such that both medial/lateral and superior/inferior components (x and z) in the principal diffusion direction are strong but, at the superior level of the region of interest considered in this study, the fibre orientations approaching SMA on average have a larger medial–lateral component, and those approaching preSMA have a larger superior/inferior component (see Fig. 4). These local differences may have a number of different causes. For example, it is possible that they reflect differences in local cortical geometry between the two functional regions. We have tried to address this question by attempting to find the boundary in T1-weighted data, which might be expected to reveal such geometric differences. The boundary was not visible. Another possibility is that these local white matter differences reflect differences in global connectivity. SMA and preSMA have a variety of cortical and subcortical connections (Luppino et al., 1993; Maier et al., 2002; Matelli and Luppino, 1996). However, one notable difference between the two regions is that preSMA maintains frontal and parietal connections via the cigulum bundle (directly inferior to the preSMA)

Table 1
Local alignment of functional boundaries on the basis of different features of the local anatomy: functional variability is measured as the standard deviation across subjects of the location along the anterior/posterior MNI-space axis of the functionally defined border between SMA and preSMA

Modality	Scope	Objective function	Features	Functional variability (mm)	Functional variability (relative)
T1w	Global	Correlation ratio	Brain boundary	4.2	1
T1w	Local	Normalised correlation	Gyral/Sulcal anatomy	9.5	2.3
T1w	Local	Mutual information (MI)	Gyral/Sulcal anatomy	9.3	2.2
T1w	Local	Manual expert 1	Gyral/Sulcal anatomy	6.4	1.5
T1w	Local	Manual expert 2	Gyral/Sulcal anatomy	5.8	1.4
DTI	Local	DTI1	Gyral/Sulcal anatomy	6.3	1.5
DTI	Local	DTI2	White matter arch.	2.6	0.6

Relative functional variability is expressed as a fraction of the functional variability computed before any local realignment is applied. Subjects were first aligned on the basis of global brain shape. The functional variability after this stage was 4.2 mm. The alignment was then refined using objective functions based either on the local gyral/sulcal anatomy or the on local white matter architecture. Only refinement on the basis of the local white matter architecture reduced the variability between subjects in the location of the white matter boundary ($P < 0.1$ by variance ratio F test).

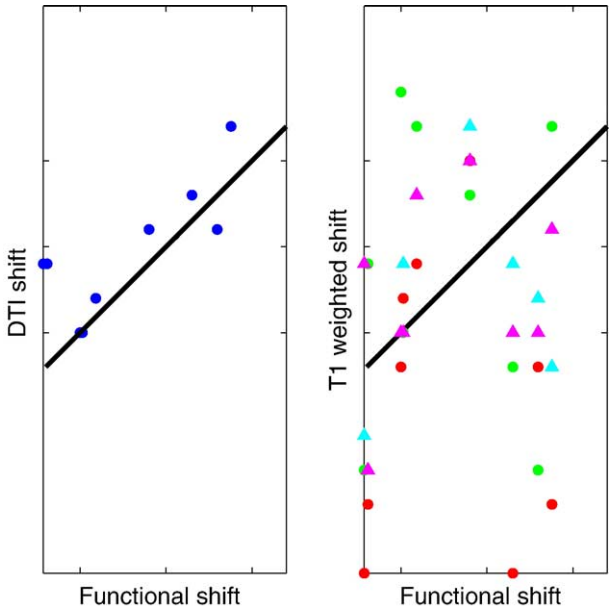

Fig. 5. Correspondence between the alignment which best matches the functional boundaries, and the best alignment achievable with DTI and structural data sets. In each plot, the x-axis shows the translation required to each subject's data to align the functional boundaries across subjects. The y-axis shows the resulting shifts after alignment to a common reference on the basis of DTI data (left) and T1-weighted data (right). Left: the results shown for the DTI data were obtained using "DTI2" objective function which is normalised for overall diffusivity. Right: the results shown for the T1-weighted data aligned both automatically and manually. Automated registration used mutual information (green circles) and normalised correlation (red circles) objective functions. Manual registrations are shown for expert 1 (cyan triangles) and expert 2 (magenta triangles). Black lines show $y = x$. In each case, a perfect functional alignment would lie along the black line. The distance between ticks is 5 mm. (For interpretation of the references to colour in this figure legend, the reader is referred to the web version of this article.)

(Johansen-Berg et al., 2004a), whereas the fibres from SMA must first circumvent the cingulum bundle before, for example, forming connections with cortico-spinal tract and lateral precentral sulcus."

Divisions in local diffusion tensor data, which are not visible in data relating to gross anatomy, have previously been reported in thalamus (Wiegel et al., 2003) but have not previously been related directly to local grey matter function. This relationship, if it proves to be generalisable to different functional regions, has important implications for future neuroimaging studies. Differences between groups in local white matter architecture may relate not to white matter integrity, but to differences in local functional organisation. Perhaps most significantly, the locations of functional activations should be compared across different subjects with respect to the local white matter architecture as well as the gross brain anatomy. Previous studies have found that cytoarchitectonic boundaries exhibit variability with respect to the gross anatomy in the normal population (Amunts et al., 1999; Rajkowska and Goldman-Rakic, 1995a,b). Information from diffusion tensor MRI could prove crucial when comparing functional responses across individuals.

We have demonstrated this concept explicitly by showing that subjects exhibit greater consistency in the location of a functional landmark after realignment according to their diffusion tensor data than after realignment according to their T1-weighted (anatomical) data but more research is required before we can assume a general correspondence between local white matter and functional architectures, and before we can use this correspondence for the alignment of functional data. The boundary between SMA and preSMA is a particularly convenient functional example: we knew from prior data that the boundary lies predominantly in the coronal plane (Zilles et al., 1996), so it was sufficient to search for only a single translation parameter to align subjects; the superior medial frontal cortex lies in a location which does not suffer from the anatomical distortions that can affect many regions in both functional and diffusion-weighted MRI scans; aligning subjects on the basis of global brain shape alone matched the functional boundary sufficiently that a very local refinement was appropriate. In order to test for this relationship in general, we would require a highly nonlinear alignment strategy and, even with such a strategy, it is likely that not every functional division would have a clear marker in the diffusion tensor data. However, even if only a few divisions were visible in general, this information has the potential to improve substantially the functional accuracy of structural brain alignments. It is also important to note that the topology of the local gyral/sulcal anatomy may confound the information available in the diffusion tensor images. The orientation of white matter fibres as they approach cortex is influenced by the orientation of the particular cortical fold.

Despite these caveats, we have demonstrated a pattern in anatomical diffusion tensor data which consistently predicts the location of a functional boundary independent of local anatomical landmarks. This finding suggests that nonlinear strategies for warping diffusion tensor images could have a great impact in future neuroimaging studies, and lends weight to the argument relating connectional architecture directly to regional brain function.

Acknowledgments

The authors would like to thank Emma Sillery, Paula Croxson, Peter Hobden and Clare Mackay for help with data acquisition; and Matthew Rushworth and Paul Matthews for invaluable advice in the preparation of the manuscript. This work was supported by the following institutions: The Wellcome Trust (HJB), the UK MRC (TEJB, HJB) and the UK EPSRC (SMS, MJ).

References

Alexander, D.C., Gee, J., Bajcsy, R., 1999. Similarity measures for matching diffusion tensor images. Proceedings of the 10th British Machine Vision Conference.

Alexander, D.C., Pierpaoli, C., Basser, P.J., Gee, J.C., 2001. Spatial transformations of diffusion tensor magnetic resonance images. IEEE Trans. Med. Imaging 20 (11), 1131–1139 (Nov).

Amunts, K., Schleicher, A., Burgel, U., Mohlberg, H., Uylings, H.B., Zilles, K., 1999. Broca's region revisited: cytoarchitecture and intersubject variability. J. Comp. Neurol. 412 (2), 319–341 (Sep).

Basser, P.J., Matiello, J., Le Bihan, D., 1994. Estimation of the effective selfdiffusion tensor from the NMR spin echo. J. Magn. Reson., B 103, 247–254.

Beaulieu, C., 2002. The basis of anisotropic water diffusion in the nervous system—a technical review. NMR Biomed. 15 (7–8), 435–455 (Nov).

Beaulieu, C., Allen, P.S., 1994. Determinants of anisotropic water diffusion in nerves. Magn. Reson. Med. 31 (4), 394–400.

Behrens, T.E.J., Johansen-Berg, H., Woolrich, M.W., Smith, S.M., Wheeler-Kingshott, C.A.M., Boulby, P.A., Barker, G.J., Sillery, E.L., Sheehan,

K., Ciccarelli, O., Thompson, A.J., Brady, J.M., Matthews, P.M., 2003. Non-invasive mapping of connections between human thalamus and cortex using diffusion imaging. Nat. Neurosci. 6 (7), 750–757.

Evans, A.C., Marrett, S., Neelin, P., Collins, L., Worsley, K., Dai, W., Milot, S., Meyer, E., Bub, D., 1992. Anatomical mapping of functional activation in stereotactic coordinate space. NeuroImage 1 (1), 43–53 (Aug).

FSL. http://www.fmrib.ox.ac.uk/fsl.

Hikosaka, O., Sakai, K., Miyauchi, S., Takino, R., Sasaki, Y., Putz, B., 1996. Activation of human presupplementary motor area in learning of sequential procedures: a functional MRI study. J. Neurophysiol. 76 (1), 617–621 (Jul).

Jenkinson, M., Smith, S., 2001. A global optimisation method for robust affine registration of brain images. Med. Image Anal. 5 (2), 143–156 (Jun).

Johansen-Berg, H., Behrens, T.E.J., Robson, M.D., Drobnjak, I., Rushworth, M.F.S., Brady, J.M., Smith, S.M., Higham, D.J., Matthews, P.M., 2004a. Changes in connectivity profiles define functionally distinct regions in human medial frontal cortex. Proc. Natl. Acad. Sci. U. S. A. 101 (36), 13335–13340 (Sep).

Johansen-Berg, H., Behrens, T.E., Sillery, E., Ciccarelli, O., Thompson, A.J., Smith, S.M., Matthews, P.M., 2004b. Functional–anatomical validation and individual variation of diffusion tractography-based segmentation of the human thalamus. Cereb. Cortex (Jul).

Luppino, G., Matelli, M., Camarda, R., Rizzolatti, G., 1993. Corticocortical connections of area F3 (SMA-proper) and area F6 (pre-SMA) in the macaque monkey. J. Comp. Neurol. 338 (1), 114–140 (Dec).

Maier, M.A., Armand, J., Kirkwood, P.A., Yang, H.-W., Davis, J.N, Lemon, R.N., 2002. Differences in the corticospinal projection from primary motor cortex and supplementary motor area to macaque upper limb motoneurons: an anatomical and electrophysiological study. Cereb. Cortex 12 (3), 281–296 (Mar).

Matelli, M. and Luppino, G., (1996). Thalamic input to mesial and superior area 6 in the macaque monkey. 372 (1), 59–87.

Matsuzaka, Y., Tanji, J., 1996. Changing directions of forthcoming arm movements: neuronal activity in the presupplementary and supplementary motor area of monkey cerebral cortex. J. Neurophysiol. 76 (4), 2327–2342.

Passingham, R.E., Stephan, K.E., Kotter, R., 2002. The anatomical basis of functional localization in the cortex. Nat. Rev., Neurosci. 3 (8), 606–616.

Picard, N., Strick, P.L., 1996. Motor areas of the medial wall: a review of their location and functional activation. Cereb. Cortex 6 (3), 342–353.

Pierpaoli, P., Basser, P.J., 1996. Toward a quantitive assessment of diffusion anisotropy. Magn. Reson. Med. 36, 893–906.

Rajkowska, G., Goldman-Rakic, P.S., 1995a. Cytoarchitectonic definition of prefrontal areas in the normal human cortex: I. Remapping of areas 9 and 46 using quantitative criteria. Cereb. Cortex 5 (4), 307–322.

Rajkowska, G., Goldman-Rakic, P.S., 1995b. Cytoarchitectonic definition of prefrontal areas in the normal human cortex: II. Variability in locations of areas 9 and 46 and relationship to the Talairach Coordinate System. Cereb. Cortex 5 (4), 323–337.

Smith, S.M., Zhang, Y., Jenkinson, M., Chen, J., Matthews, P.M., Federico, A., De Stefano, N., 2002. Accurate, robust, and automated longitudinal and cross-sectional brain change analysis. NeuroImage 17 (1), 479–489.

Tanji, J., 2001. Sequential organization of multiple movements: involvement of cortical motor areas. Annu. Rev. Neurosci. 24, 631–651.

Wiegell, M.R., Tuch, D.S., Larsson, H.B.W., Wedeen, V.J., 2003. Automatic segmentation of thalamic nuclei from diffusion tensor magnetic resonance imaging. NeuroImage 19 (2 Pt 1), 391–401 (Jun).

Woolrich, M.W., Ripley, B.D., Brady, M., Smith, S.M., 2001. Temporal autocorrelation in univariate linear modeling of FMRI data. NeuroImage 14 (6), 1370–1386 (Dec).

Zilles, K., Schlaug, G., Geyer, S., Luppino, G., Matelli, M., Qu, M., Schleicher, A., Schormann, T., 1996. Anatomy and transmitter receptors of the supplementary motor areas in the human and nonhuman primate brain. Adv. Neurol. 70, 29–43.